Available online at www.sciencedirect.com
SCIENCE DIRECT®
Renewable Energy 29 (2004) 2195–2216
RENEWABLE ENERGY
www.elsevier.com/locate/renene

Modeling anti-islanding protection devices for photovoltaic systems

Mei Xu [a], Roderick V.N. Melnik [a,b,*], Uffe Borup [c]

[a] *Faculty of Science and Engineering, Mads Clausen Institute, University of Southern Denmark, Grundvigs Alle 150, DK-6400 Soenderborg, Denmark*
[b] *College of Engineering and Science, Computational Analysis and Modeling, Louisiana Technical University, P.O. Box 10348, 6000 W. Arizona Avenue, Ruston, LA 71272, USA*
[c] *PowerLynx A/S, Ellegaardvej 36, DK-6400 Soenderborg, Denmark*

Received 11 November 2003; accepted 22 April 2004

Abstract

Applications of grid-connected photovoltaic systems are rapidly expanding, providing a viable technology for renewable energy resources. Such systems are utility interactive and one of the major difficulties in their efficient use is related to islanding phenomena connected with a possibility of supplying surplus power back to the utility grid. In detecting and preventing such situations, anti-islanding protection devices play a paramount role. In this paper, we analyze the existing techniques in order to identify a methodology with an optimum combination of characteristics. We implement the chosen methodologies in SIMULINK. Major attention is given to the phase jump detection method (PJD), and to the slip mode frequency shift method (SMS) for which we provide a detailed description of our SIMULINK implementations and their evaluations performed on the basis of their non-detection zones. We develop an experimental iterative scheme to validate the results of computational experiments obtained with the developed models, and report the results of several computational tests.

Keywords: Grid-connected photovoltaic systems; Renewable energy technologies; Islanding; Modeling; Non-detection zone

* Corresponding author. Tel.: +1-318-257-3198; fax: +1-318-257-3823.
E-mail address: rmelnik@latech.edu (R.V.N. Melnik).

0960-1481/$ - see front matter © 2004 Elsevier Ltd. All rights reserved.
doi:10.1016/j.renene.2004.04.005

1. Introduction

Grid-connected photovoltaic (PV) systems continue to attract an increasing interest, in particular, in the form of photovoltaic arrays as an alternative source of energy. Such systems use solar energy to generate electricity, and they can be efficiently used as a power source for domestic use. One of the most important issues in the application of these and other dispersed power systems is the development of efficient protection techniques against a phenomenon known as islanding as well as against other "run-on" phenomena [19]. Indeed, in applications, PV systems have to be connected to a utility power grid, and hence, one has to deal with utility interactive PV systems, because both the PV system and the grid supply power to the load. If the power generated by the PV system is greater than the total needs of the entire system, the excess power will be fed back into the grid; otherwise, the power will be drawn from the grid to meet the requirement of the load.

Islanding of a grid-connected PV system occurs when a section of the utility system containing such a PV system is disconnected from the main utility voltage source; however, the PV system continues to feed the utility lines in the isolated section known as an island [15]. Such isolated islands may cause a serious danger to the personnel who may consider the load as inactive, while in reality, the PV system may feed power to utilities. They may also substantially complicate the normal reconnection of the utility network due to a damage made to the load in the island itself. Furthermore, for those utility customers located in the island, the connected equipment may also be damaged, because the supplying power will not be able to maintain the required power quality [11,12,17]. For these reasons, the islanding phenomenon is considered as one of the most important issues in designing PV systems, and in maintaining reliable utility grid operation [18].

The existing methodologies for islanding detection and prevention can be divided into two categories: active methods and passive methods [5,7,10,13,14]. In applications, each specific methodology has its own advantages and drawbacks. Therefore, in designing anti-islanding protection devices, both mathematical theory and measurements of PV systems play an important role in the success of the entire process. In this paper, our goal is to analyze, implement, and test methodologies that are most promising for this process. The paper is structured as follows. In Section 2, we give a brief overview of the existing methodologies with the aim of identifying two most promising techniques for subsequent analysis. In Section 3, we highlight the main features of the islanding network used as a prototype in further discussion. Section 4 is devoted to the construction of models for the two chosen methodologies. The main characteristic of the effectiveness of anti-islanding methods is their non-detection zone (NDZ), which is evaluated and compared in Section 5. A scheme for the experimental validation of the developed models is discussed in Section 6 by considering a case with one load combination. In Section 7, we apply that scheme to compare experimental results with the results of computations obtained with the developed models. Conclusions are given in Section 8.

2. Comparison of anti-islanding methodologies and network analysis: basic assumptions and specifications

It is commonly agreed in the literature (e.g., [16]) that in order to be effective, an islanding prevention method should be able (a) to detect islanding and disconnect the PV system from the utility (this should be possible to achieve in different environments, with different initial states of the system, the multiple inverter case situations, etc.), (b) to detect islanding fast enough by guaranteeing safety, reliability, and integrity of the entire system, and (c) to disconnect the PV system only when actual islanding happens that is when the grid supply is disconnected but the local network voltage and frequency remain within regulation limits (e.g., [14]).

A number of methodologies have been developed in the literature with the aim achieving the above goals. Based on the literature review, in particular [3–6,8,9,16], we have analyzed the most promising methodologies, both passive and active, typical for inverters. The methods that require implementing communication techniques (e.g., based on signal processing, supervisory control, etc.) between the grid and the PV system have remained outside the scope of the present paper. The methods that have been analyzed include: under/over voltage and under/over frequency (OUV/OUF), voltage phase jump detection (PJD), and harmonic detection in the group of passive methodologies, as well as impedance measurement, slip mode frequency shift (SMS), active frequency drift method (AFD), active frequency drift with positive feedback (AFDPF), mains monitoring units with allocated all-pole switching devices connected in series (MSD or ENS) in the group of active methodologies, among others.

Most of the methods that we are interested in here can be compared based on a technique developed in [16] which is well established for standard protection systems. Let us denote the power coming to a certain node "a" of the grid-connected utility interactive system from the PV system as $P_{pv} + jQ_{pv}$ (with P and Q denoting the real and reactive powers, respectively). The power coming from that node to the load is denoted as $P_{load} + jQ_{load}$. Hence, the difference between the two is easily defined as [4]

$$\Delta P = P_{load} - P_{pv} \quad \Delta Q = Q_{load} - Q_{pv}. \tag{1}$$

It is the values of ΔP and ΔQ that determine the behaviour of the system. In particular, when the utility relay or breaker is open, both these values are zero, while the analysis of an isolated system will be essentially determined by their values just before that relay opens while forming an island. Following [16], we denote these values as ΔP^- and ΔQ^-. Since these values may fall into a non-detection zone of the method used for islanding detection, we need to analyze how close these values are to zero.

There are several different cases to consider. If $\Delta P^- \neq 0$, the standard OUV/OUF method can be applied. This method includes four standard relays: an overvoltage relay, an undervoltage relay, an overfrequency relay, and an underfrequency relay. The abnormal voltage or frequency will cause the relays open so that the inverter is disconnected from the grid [2]. The drawback of this approach

is related to the situation where $\Delta Q^- \neq 0$, in which case this methodology cannot guarantee the islanding protection. On the contrary, the PJD methodology can effectively prevent islanding in the case where $\Delta P^- \neq 0$. The methodology can be quite effective in practice, and we have chosen this methodology for our further analysis as a representative example from the group of passive methodologies. Note also that the methodology works also in the multi-inverter case (in particular, when all inverters use the same anti-islanding prevention scheme).

There is experimental evidence to suggest (see [16] and references therein) that in the group of active methodologies the SMS methodology is highly effective and can work efficiently even in multi-inverter situations. If phase conditions are met (which can be achieved by an *RLC* makeup of the load, as shown in Fig. 1), this method works for any ΔP^-. It works well for the case of $\Delta Q^- \neq 0$, as well as for the case of $\Delta P^- = \Delta Q^- \approx 0$ (no matter whether we deal with purely resistive loads or resonant *RLC* loads). It is this method that will be analyzed further in this paper with a model and its SIMULINK implementation discussed in Sections 4–7.

In order to establish a mathematical model of prototype anti-islanding devices for PV systems based on PJD and SMS methodologies, we make the following simplifications. In what follows, a PV inverter is considered as a current source and the utility grid is simplified as a voltage source. In our representation of the utility interactive PV system, we follow [16] (see also references therein). This representation is given schematically in Fig. 1, and it contains all basic components present in standard PV system/utility feeder configurations.

The analysis of an islanding network is performed under the assumption that the grid can supply sufficient power to the load. In other words, we assume that as long as the grid is connected, we have the following relationship satisfied:

$$P_{\text{grid}} = P_{\text{load}}, \qquad V_{\text{a}} = 230\ \text{V}, \qquad f_{\text{a}} = 50\ \text{Hz}, \tag{2}$$

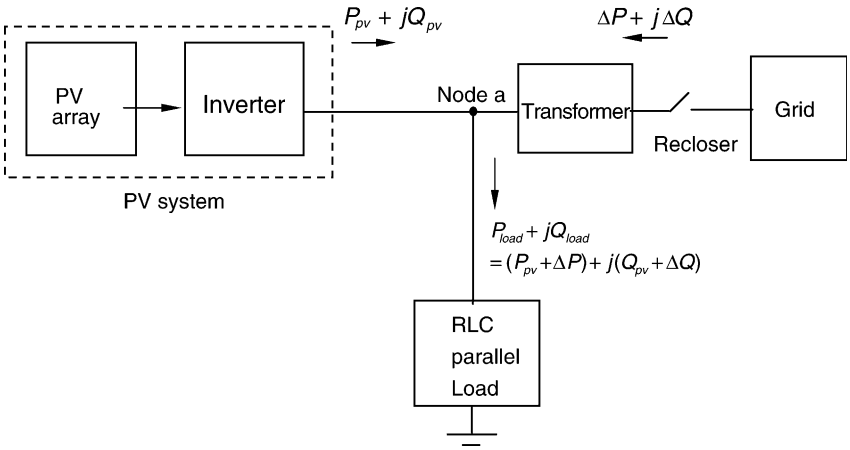

Fig. 1. Schematic configuration of the PV system/utility.

where P_{grid} is the power supplied by the load, V_a is the load voltage, and f_a is its frequency. While the grid is connected, the frequency of PV current is assumed to be the same as that of the load voltage (in our case, $f_{pv} = f_a = 50$ Hz). After the grid is disconnected, the frequency of PV shifts to follow the load voltage, and in this case, we have $f_{pv} \neq 50$ Hz. We denote the phase angle of inverter current by θ.

Note also that the power factor (PF) of the inverter depends on a specific anti-islanding method in use. For most passive methods, PF of the inverter is one, while for active methods, PF may change with respect to the frequency. Indeed, the real power of the load remains the same for the inverter, no matter whether the real power is matched or not before islanding, but actual powers could be different. This may be formalized by the following model:

– immediately before the islanding, we have the following relationship:

$$P_{load} + jQ_{load} = (P_{pv} + \Delta P) + j(Q_{pv} + \Delta Q) \tag{3}$$

– in the islanding situation, we have:

$$P_{load} = I_{pv} V_{load} \cos\theta_{load} = P_{pv}, \quad I_{pv} = \frac{P_{pv}}{V_{load}\cos\theta_{load}}, \tag{4}$$

where V_{load} is the real time root mean square (RMS) voltage measured from the load, Q is the reactive power, for which the (lagging) PF is positive, and θ_{load} can be interpreted as the angle of the power factor of the load.

3. Implementation of the PJD methodology for islanding detection

Our major goal in the subsequent sections is to implement and computationally analyze the SMS methodology. In this section, we start our discussion from the PJD method as a representative method from Group I. As we would see, there are several subsystems that are common for both SMS and PJD methodologies. In Fig. 2, we provide the model of the entire system with built-in PJD methodology for islanding protection.

Here, we model the load as a parallel RLC makeup. Certainly, in reality, the situation is more complicated. However, experimental test results and theoretical evidence (e.g., [2]) show that this simple model should work well in the prediction of worst-case islanding test conditions. The parallel RLC in our model can be presented by the following transfer function:

$$Z = \frac{1}{\frac{1}{R} + \frac{1}{Ls} + Cs} = \frac{RLs}{RLCs^2 + Ls + R}. \tag{5}$$

It is straightforward to implement the subsystem "$1/Z$", but in doing so, one has to note that the transfer function cannot be written as the reciprocal of (5), because in implementing the standard transfer function block, the order of the numerator cannot be larger than that of the denominator. Instead, one can easily

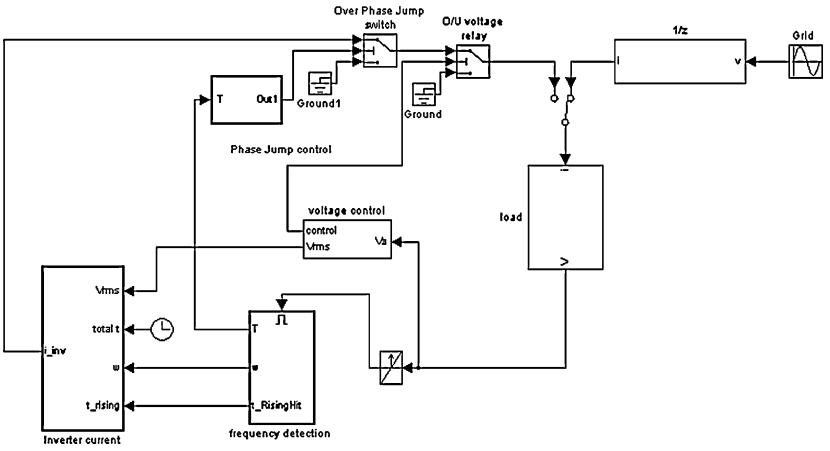

Fig. 2. The system model with PJD method.

observe that $1/Z$ can be rewritten as follows:

$$\frac{1}{Z} = \frac{1}{R} + \frac{1}{Ls} + Cs = \frac{RLCs^2 + Ls + R}{RLs^2} s = G(s)\frac{\mathrm{d}u}{\mathrm{d}t}. \tag{6}$$

The representation of $1/Z$ in form (6) allows us to realize this subsystem by connecting a "transfer function" block (with the second order polynomials in the numerator and denominator which is a legal expression for SIMULINK implementation) and a "differential" block. The block diagram is implemented in SIMULINK in a straightforward manner and is shown in Fig. 3.

Next, we need to implement the frequency detection block. The load voltage is taken for this purpose as an approximate sine wave. The information on the detection period is recorded each time instance for which voltage crosses zero from negative to positive values. Then, the time interval between the two successive time instances is a period, and the frequency can be found by calculating the reciprocal of the period. The implementation of the frequency detection block is given in Fig. 4.

Note that the above three subsystems also provide a basis for both model implementations with SMS methodology and with standard OUV/OUF method. In Section 5, we use the latter for comparisons based on non-detection zone evaluation. The differences between three methodologies that we analyzed are reflected in the

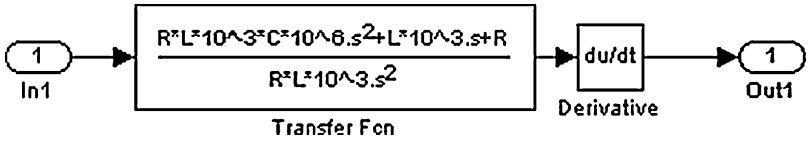

Fig. 3. Block diagram of "$1/Z$" subsystem.

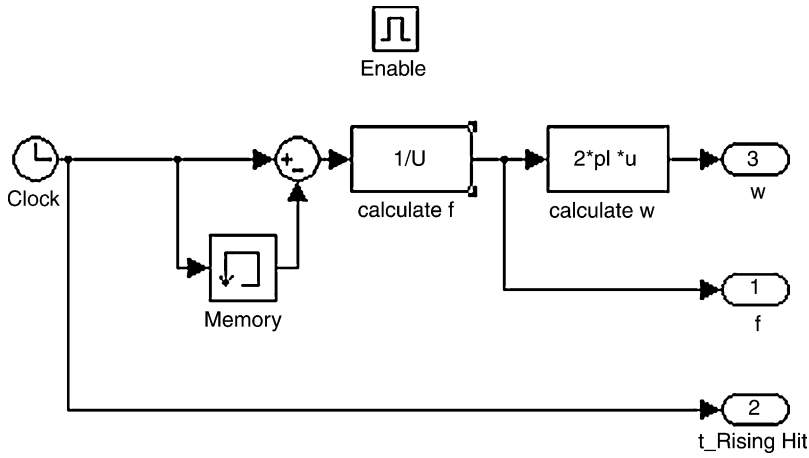

Fig. 4. Subsystem of "frequency detection".

implementation of current generating and trip functions. Indeed, recall that for a unity power-factor inverter, the current and voltage are in phase. In the implementation, the current starts at a positive zero crossing of voltage, which is the time instance when the voltage rises to zero from being negative, and ends at the next positive zero crossing. At the same time moment, a new current period begins [17]. Hence, one can observe that the frequency of current is the same as the voltage frequency, and the current frequency can be different in each new period. A graphical interpretation of this explanation is given in Fig. 5.

To recast the observations in Fig. 5 in a formal mathematical way, we write the current in the following form:

$$i_{\mathrm{pv}} = I_{\mathrm{m}} \sin\omega_{\mathrm{a}}(t - t_1), \tag{7}$$

where i_{pv} is the inverter current, I_{m} is the amplitude of the inverter current, ω_{a} is the angular frequency of the load voltage V_{a}, t_1 is the time moment of positive zero crossing of V_{a}, and t is the simulation time, which is counted from start to the current time.

Shortly after islanding conditions arise, frequency of the voltage changes, and, as we have explained above, each subsequent frequency may be different from the previous one. The methodology has been implemented in SIMULINK, and we present this implementation in Fig. 6. Note that we use a switch to jump over the time interval corresponding to the situation where the root mean square value of the load voltage is equal to zero, i.e. $V_{\mathrm{rms}} = 0$. This switch begins to operate in the case where the simulation has just been started; otherwise, the system produces a warning "divided by zero".

In Fig. 6, the power factor of load is found according to Eq. (8):

$$\theta = a\tan\left[\left(\frac{1}{\omega L} - \omega C\right)R\right]. \tag{8}$$

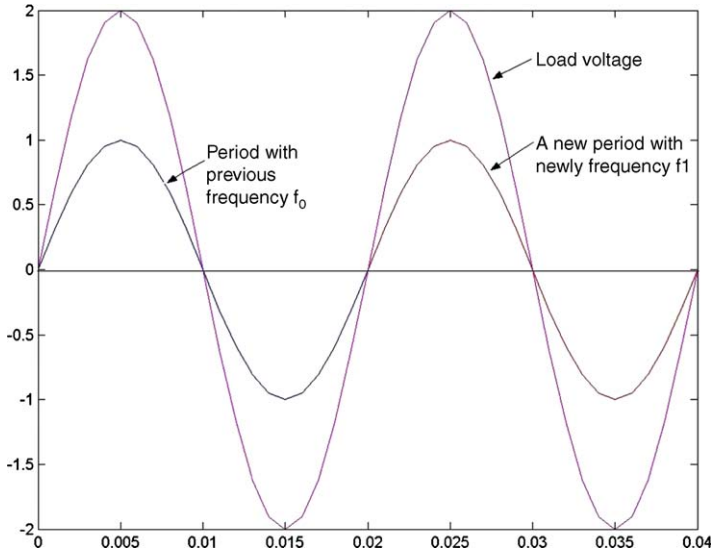

Fig. 5. The relation between inverter current and load voltage.

For convenience, we set the input units of L and C as millihenry and microfarad, so that in the block "PF of load", L and C are multiplied by 1×10^{-3} and 1×10^{-6}, respectively.

In Fig. 7, we present the block diagram of the "voltage control" subsystem. It contains several major parts. The part containing a sequence of blocks from the input block to the "calculate V_{rms}" block is used here to calculate V_{rms}. The next part, presented in Fig. 7, generates a control signal according to the supplied voltage. The subsequent part is the "stop after 4 abnormal periods" subsystem, which ensures that the inverter stops when the islanding does occur. The algorithm imple-

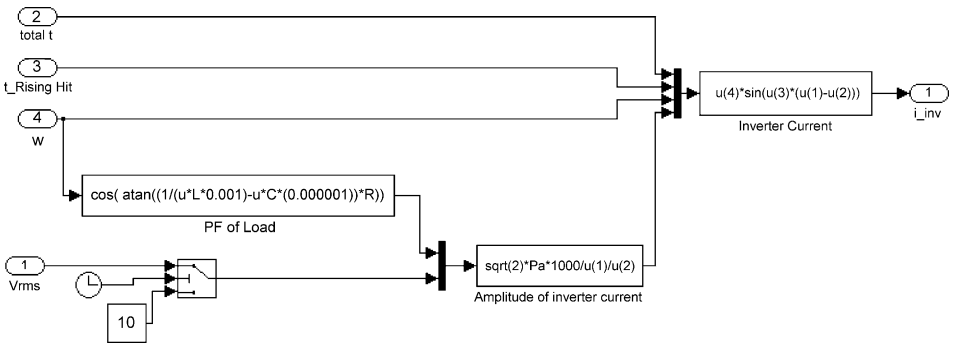

Fig. 6. Implementation of the inverter current block with PJD method.

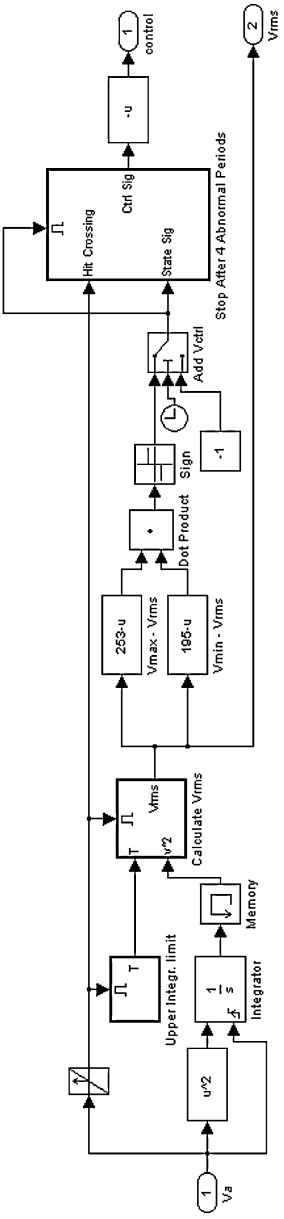

Fig. 7. Block diagram of the "voltage control" subsystem.

mented in this part tests four successive periods: if all of them are abnormal, the situation is considered as such where the islanding phenomenon does take place. This part is explained in detail in Fig. 8(a)–(c).

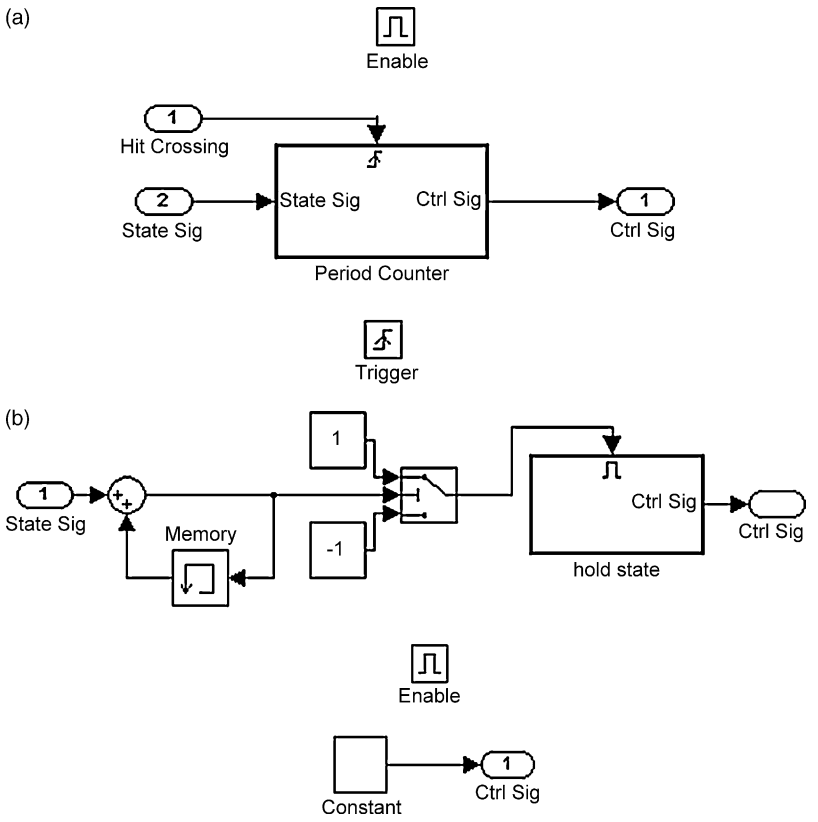

Fig. 8. Nested subsystems in the "stop after 4 abnormal periods" part. (a) Block diagram of the "stop after 4 abnormal periods" subsystem. (b) Block diagram of the "period counter" subsystem. (c) Block diagram of the "hold state" subsystem.

Finally, the "phase jump control" and "voltage control" blocks are used to generate a signal to stop the inverter when islanding is detected. The implementations of these blocks are shown in Figs. 9 and 10, respectively.

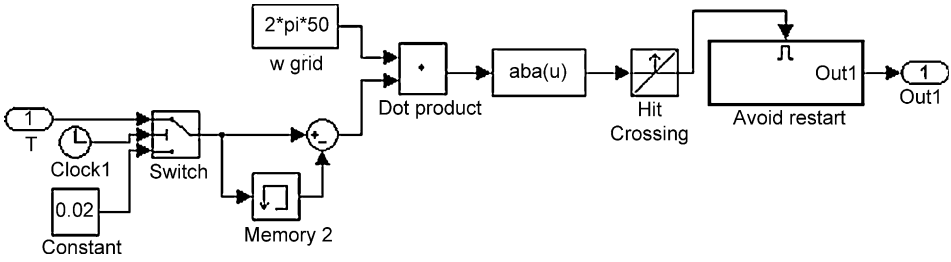

Fig. 9. Block diagram of the "phase jump control" subsystem.

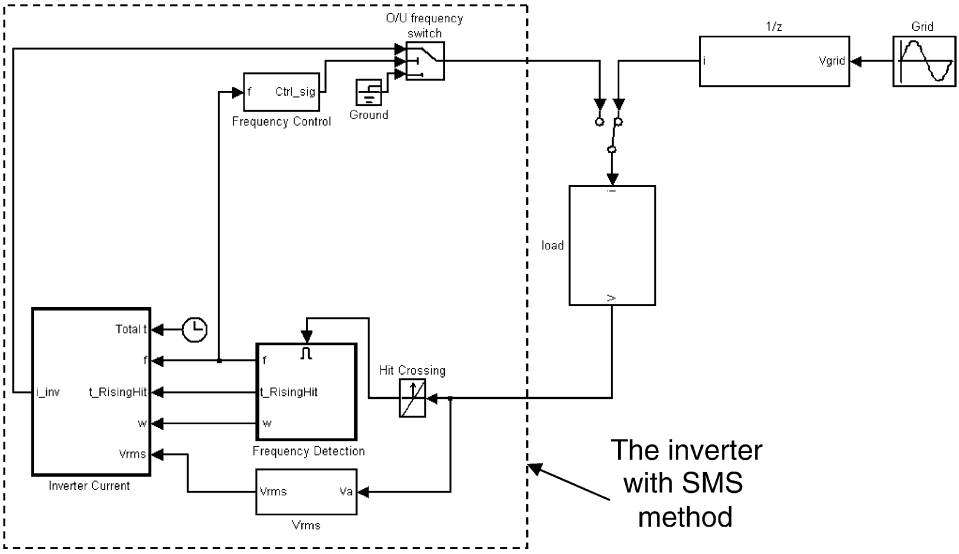

Fig. 10. System model with SMS method.

In Fig. 9, the angular frequency of the grid voltage is found as follows:

$$\omega = 2\pi f_{\text{rate}} = 2 \times \pi \times 50. \tag{9}$$

The block diagram of the "avoid restart" subsystem is the same as the one shown in Fig. 8(c). This completes the model construction for the entire system with PJD method. Now, we are in a position to proceed to a more complicated case related to the implementation of our active methodology for islanding detection and prevention.

4. Implementation of the SMS method for islanding detection

We have implemented the SMS method for the entire system by using modeling tools of SIMULINK. The result is presented in Fig. 10. The system consists of a number of subsystems, some of which are intrinsic to the group of active methods, while the others can find their counterparts in the passive methodologies.

Note, in particular, that subsystems called "grid", "frequency detection", "load" as well as the "$1/Z$" subsystem are modeled in absolutely the same way as their analogues in the PJD methodology. One of the intrinsic features in our implementation of this active method, which is not present in the passive PJD methodology, lies in the fact that the PF of inverter changes with respect to the frequency. Schematically, this phase–frequency relation is represented in Fig. 11.

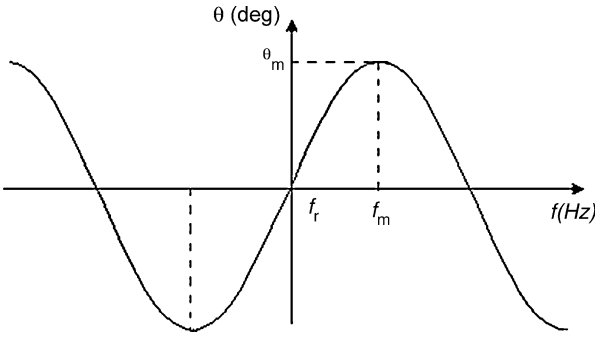

Fig. 11. SMS sinusoidal frequency shift [15].

In this case, the phase–frequency relation can be expressed by a simple sinusoidal dependency as follows:

$$\theta = \theta_{\mathrm{m}} \sin\left[\frac{\pi(f - f_{\mathrm{r}})}{2(f_{\mathrm{m}} - f_{\mathrm{r}})}\right], \tag{10}$$

where θ_{m} is the maximum phase angle of the inverter, f_{r} is the rated frequency (the frequency of normal operation), and f_{m} is the frequency corresponding to the maximum phase angle of the inverter. Frequency limits have been taken as follows: f_{m} has been set at 51 Hz, and f_{r} has been set at 50 Hz. We consider the worst quality factor of load ($Q_{\mathrm{f}} = 2.5$) and take θ_{m} to be 10°. The inverter current is modeled by using the following dependency

$$i_{\mathrm{pv}} = I_{\mathrm{m}} \sin\omega_{\mathrm{a}}[(t - t_1) + \theta] = \frac{\sqrt{2}P_{\mathrm{pv}}}{V_{\mathrm{rms}}\cos\theta_{\mathrm{load}}} \sin[(t - t_1) + \theta], \tag{11}$$

where I_{m} is the amplitude of the inverter current, ω_{a} is the angular frequency of the load voltage V_{a}, and t_1 is the time moment that corresponds to the onset of positive zero crossing of V_{a}.

A natural simplification of our model follows from the fact that no stable running state is needed in islanding. Hence, the phase–frequency curve can be approximated quite well by a straight line as follows:

$$\theta = 15 \times (f - 50). \tag{12}$$

In order to cover the islanding cases typical for the inverter with characteristic curve presented in (10), the biggest slope of Eq. (10) on the interval of 49–51 Hz is chosen as the slope of the straight characteristic line. The advantage of Eq. (12) is obvious: it allows for an easier implementation compared to the original sinusoidal representation of the phase angle–frequency relation.

In Fig. 12, we present a complete block diagram of the "inverter current" subsystem. In this diagram, Eq. (12) is applied as a look-up table, where θ is determined by the input frequency. The current amplitude is calculated according to Eq. (4). The time moments of positive zero crossings are measured in the

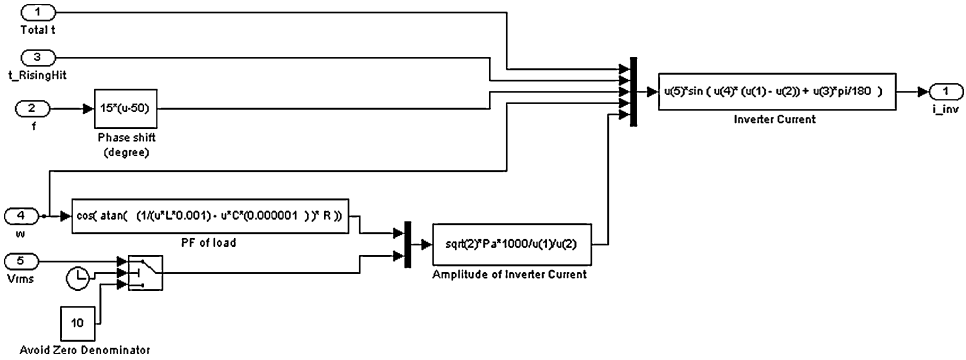

Fig. 12. The block diagram of the "inverter current" subsystem.

"frequency detection" subsystem. The value of V_{rms} is calculated by the "V_{rms}" subsystem (see Fig. 13). The difference from the "voltage control" subsystem implemented in the PJD method is that the "V_{rms}" subsystem in our present situation does not generate a control signal.

Having described the PJD methodology in detail in the previous section, the only thing that is left for the SMS method is to implement a monitoring function of the load frequency. This implementation is presented in Fig. 14.

Our last comment in this section is related to an observation that in the case where the damped frequency in islanding is near rated grid frequency (since the load frequency is detected all the time), we have the damped frequency that is in the normal range of operation. Hence, in contrary to what we want to achieve, the model will start the inverter again in this case after a very short time interval. To prevent the inverter from operating in the above situation, we have implemented a "disable restart" subsystem (see Fig. 14). This subsystem always outputs a stop signal starting from the time moment when the first frequency trip occurs.

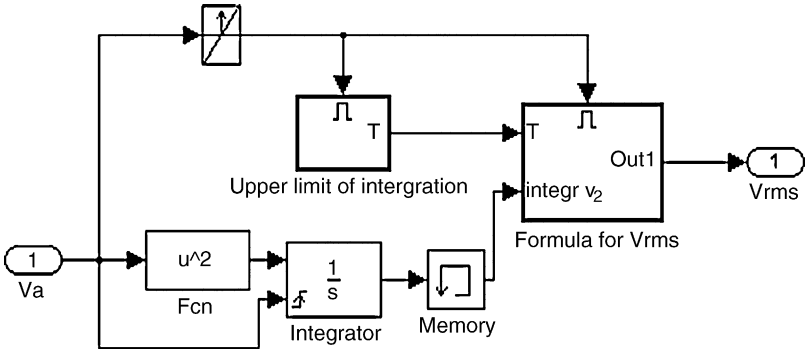

Fig. 13. Block diagram of the "V_{rms}" subsystem.

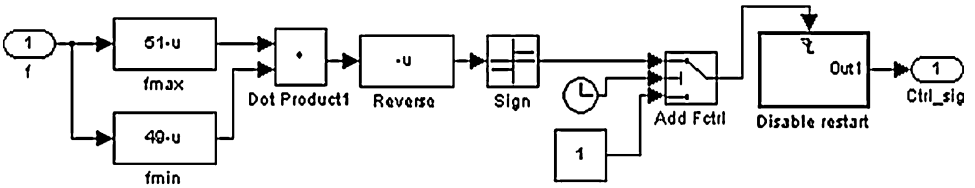

Fig. 14. Subsystem of the "frequency control".

5. Evaluating main characteristics of anti-islanding method quality

A major characteristic that determines the quality of any anti-islanding methodology is its non-detection zone. The aim of this section is to present non-detection zones produced by the methodologies developed and implemented in the previous sections. For the purpose of evaluating these non-detection zones, first we specify all necessary parameters of the system used in our evaluation. According to the IEEE definition for a non-islanding inverter [1], we know that the closely matched load case has a quality factor (denoted by Q_f) of 2.5 or less. All evaluations of non-detection zones presented below are obtained with $Q_f = 2.5$.

The quality factor is defined by the following relationship:

$$Q_f = R\sqrt{\frac{C}{L}}. \tag{13}$$

Taking into account that in the resonant case, the angular frequency is

$$\omega = \frac{1}{\sqrt{LC}}, \tag{14}$$

we arrive at the following representation of the quality factor:

$$Q_f = \frac{R}{\omega L}. \tag{15}$$

The selected Q_f of 2.5 equates to the power factor of 0.37. Indeed, in our case, the power factor is determined by the uncompensated RL load, while the capacitor can be seen as a shunt for improving the power factor. The relationship connecting PF and Q_f can be written as follows (e.g., [1]): $PF = \cos(a\tan(Q_f))$. Due to the fact that the power factor increases when Q_f decreases, we conclude that the IEEE requirement of $Q_f = 2.5$ (or less) equates to uncompensated power factors from 0.37 to unity. This will cover all practical distribution line power factors [1].

Fig. 15 is the NDZs of the PJD method, the SMS method and the OUV/OUF method, which are evaluated under the above conditions.

To make Fig. 15 easy to understand, some abbreviations are explained here:

OFR—overfrequency relay,
UFR—underfrequency relay,

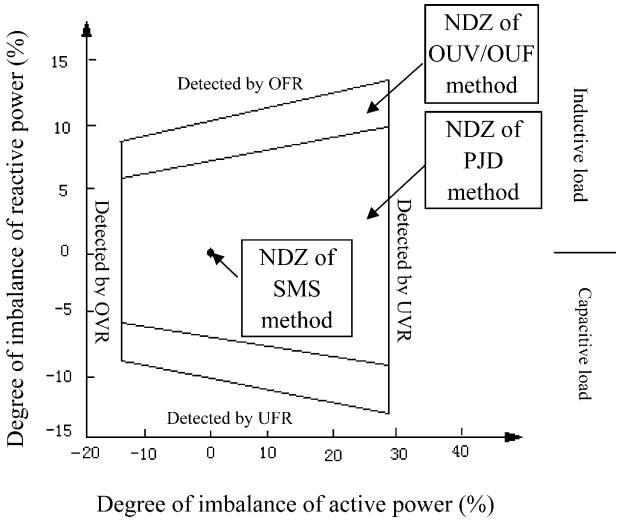

Fig. 15. NDZs of PJD, SMS and OUV/OUF methods [1].

OUR—overvoltage relay,
UVR—undervoltage relay.
The degree of imbalance of reactive power is presented as $(Q_{load} - Q_{inv})/P_{load} \times 100\%$
The degree of imbalance of active power is presented as $(P_{load} - P_{inv})/P_{load} \times 100\%$

In Fig. 15, we use the following notation: P_{load} is the active power of the load, P_{inv} is the active power of the inverter, Q_{load} is the reactive power of the load, and Q_{inv} is the reactive power of the inverter. The NDZs presented in Fig. 15 have been evaluated in the case of imbalance in both active power and active power.

First, we note that the NDZ of the standard OUV/OUF method is used here as a starting point for further improvements. In Fig. 15, this area is the outer trapezoid. Then, we present the NDZ of the PJD method, which is represented in Fig. 15 by the inner trapezoid. We observe that the PJD method reduces the NDZ of the standard OUV/OUF, in particular in the case where the reactive power is not matched, as can be judged upon from Fig. 15. The underlying difficulty with the PJD methodology, however, lies with the fact that it is extremely difficult to define a reliable phase jump threshold (indeed, even without any islanding conditions, the start of big motors may cause abnormal phase shift) (Table 1).

Finally, we note that from a theoretical point of view, the NDZ of the SMS methodology is a single point, which corresponds to the case where both real power and reactive power are perfectly matched. In this ideal case, there is no power drawn from the grid. Even when there is no connection of the grid to the load, the load still works normally. In other words, the existence of the grid has no

Table 1
The implemented methods and their thresholds

Method	Threshold			
	Upper voltage limit (V)	Lower voltage limit (V)	Upper frequency limit (Hz)	Lower frequency limit (Hz)
OUV/OUF method	253	195	51	49
PJD method	253	195	Phase jump threshold: 3°	
SMS method	51	49	–	–

effect on the frequency or the voltage of the load. Therefore, there is no frequency shift or voltage variation. In this case, the threshold of frequency should be much easier to set compared to the passive methods like the PJD. Note that in reality, the output power of the inverter varies (e.g., as a result of different weather/sunlight conditions) as does the load power. Under these conditions, a situation where real and reactive powers are perfectly matched is practically impossible which leads to a very high efficiency of the SMS methodology.

6. Experimental setup and iterative experimental scheme

In this section, we describe an experimental scheme used in testing our model for the SMS methodology that has been developed in the previous sections. All major parts of the experimental setup can be seen in Fig. 16, including the power supply, oscilloscope, DC–DC transformer, computer, capacitors, and inductors (resistors are not presented in the figure). The block diagram of this experimental setup is presented in Fig. 17. In this figure, the DC power supply is used to simulate the solar panel providing DC power to the inverter.

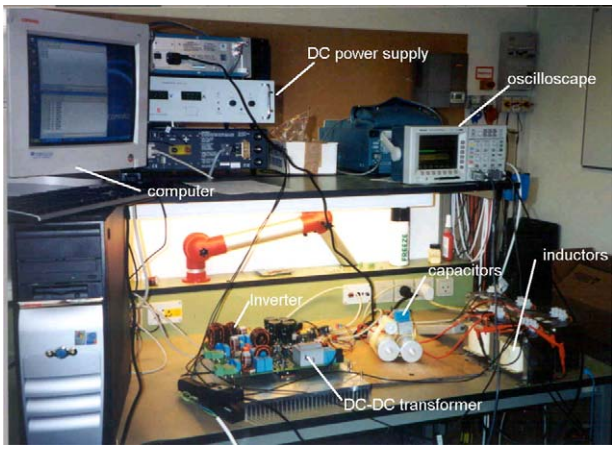

Fig. 16. Experimental equipments used in the tests.

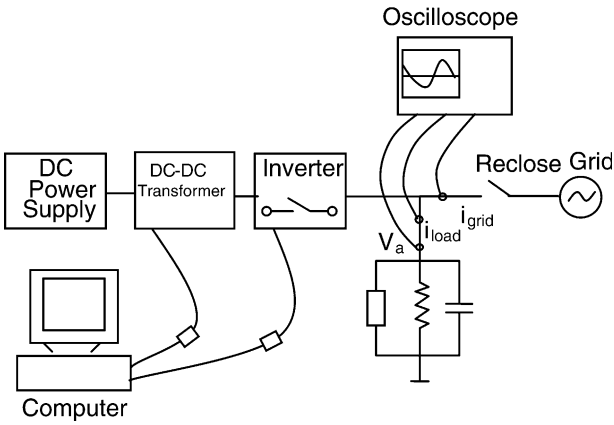

Fig. 17. Block diagram of the experimental setup.

In the experiment, the input voltage of the inverter was required to be 340 V, and hence a DC–DC transformer was needed to raise the voltage. The inverter and the grid were connected by an *RLC* load, and, in its turn, the grid was connected to the load through a recloser. The latter was viewed as a breakpoint, which can cause islanding on the grid. Furthermore, there was a built-in switch in the inverter for stopping the inverter when islanding was detected. The computer (as seen in Fig. 16) was used to control the DC–DC transformer and inverter. The transformer and inverter run independently after the initial start-up. One current probe measured the inverter current, while the other measured the grid current. A voltage meter measured the load voltage. Note that both the current probes and the voltage meter were connected with the oscilloscope (shown in Fig. 16) through different channels.

The following specifications were used for experimental tests: $R = 55\ \Omega$, $L = 80.3 \times 10^{-3}$ mH, $C = 90.2\ \mu$F. The load was capacitive and the quality factor was 2.2. The results of these experiments were used for comparisons with the results obtained with the developed model. This is discussed in the next section. We conclude this section by presenting an iterative scheme (Fig. 18) that schematically describes the entire procedure of our experimental tests.

7. Computational results and comparisons with experiments

In this section, we report two groups of computational experiments performed with the developed model. In the first group, our aim is to demonstrate that the implemented SMS methodology is superior over the standard OUV/OUF method. In the second group of computational tests, we evaluate detection times for both of these methodologies. In both cases, we compare the results obtained with the model and the experimental results performed according to the scheme described in

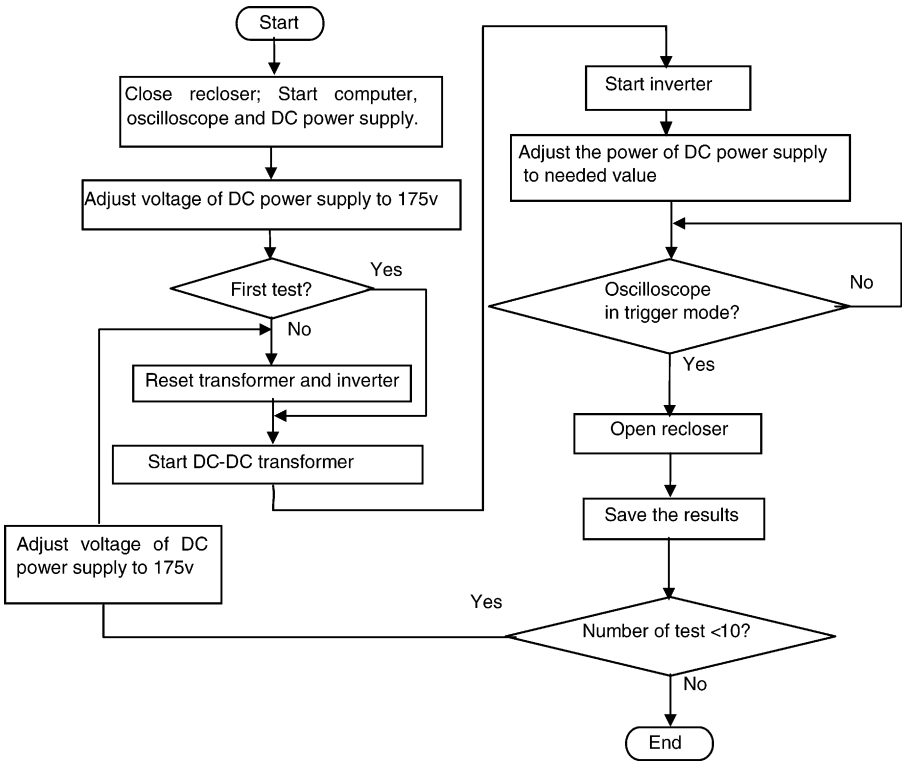

Fig. 18. The iterative experimental procedure.

the previous section. Because of the setup in the experiments, the inverter power cannot be explicitly measured, while it can be obtained approximately by excluding the internal power consumption of inverter from DC power. By experience, 8% power decay of the inverter is used in the following computations.

7.1. Computational experiment 1

The implemented models for the OUV/OUF and SMS methods have been compared under the conditions specified below:

- DC power: $P_{\mathrm{DC}} = 3.1\ \mathrm{A} \times 293\ \mathrm{V} \approx 908\ \mathrm{W}$.
- The power of inverter: $P_{\mathrm{inv}} = P_{\mathrm{DC}}(1 - 0.08) \approx 835\ \mathrm{W}$.
- The power of load: $P_{\mathrm{load}} = (220\ \mathrm{V})^2/55\ \Omega \approx 880\ \mathrm{W}$.
- Degree of imbalance: $\Delta P/P_{\mathrm{load}} = 835\ \mathrm{W} - 880\ \mathrm{W}/880\ \mathrm{W} \approx -5\%$.

Under these conditions, the standard OUV/OUF method fails to detect islanding. However, as we demonstrate in Fig. 19, the SMS method can successfully

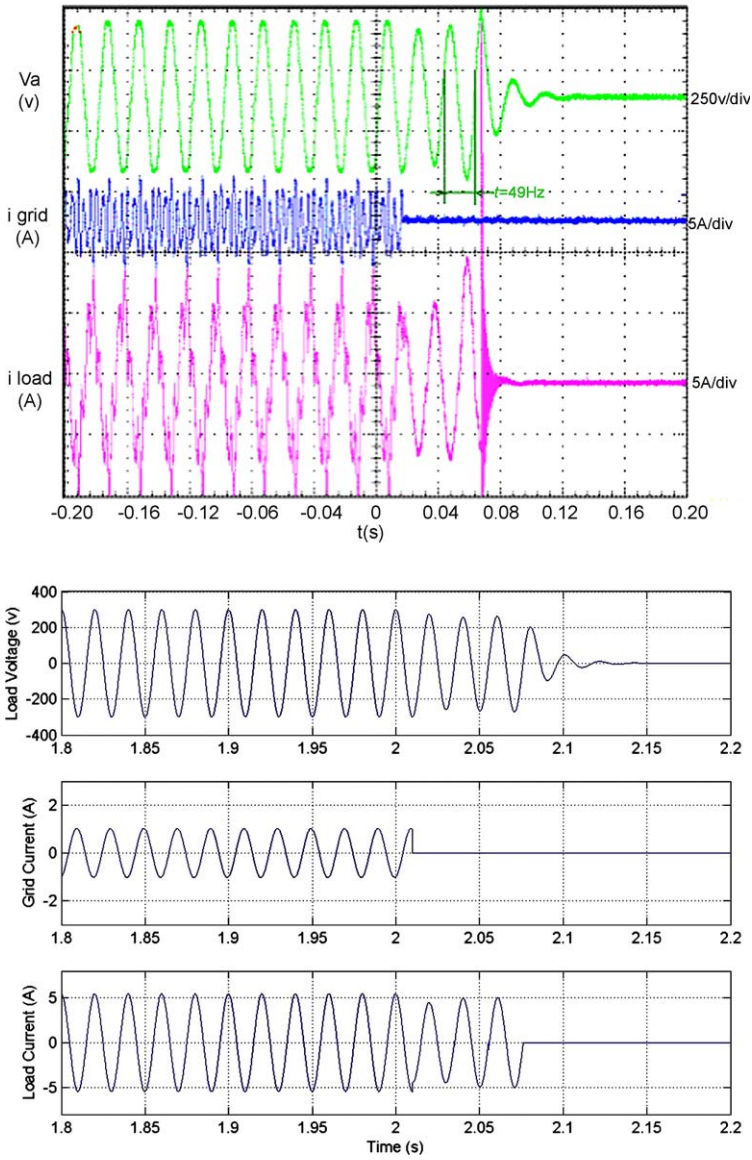

Fig. 19. Islanding detected by the SMS method in the case P_{inv} is 5% less than P_{load}.

detect islanding conditions. The results are presented alongside with the experimental results obtained under the specifications described before. Since the power of the inverter is less than that of the load, the voltage and current should drop in islanding. This phenomenon is observed in both experiment and simulation. For convenience, we define the main divisions at the triggering point at time zero (the

time before that is negative and the time after it is positive), with the time units given in seconds. The detection time determined by our experimental equipment is about $(0.070 - 0.016) = 0.054$ s, while the detection time determined by our computational algorithm is $(2.075 - 2.010) = 0.065$ s. Given the inaccuracy in measurements caused by power variations and other factors, experimental and computed results are in good agreement.

Note that not only does the model predict the detection time quite well, but it gives also the same changing tendency in current and voltage as obtained from the experimental results. This happens in the situation where the standard methodologies typically fail.

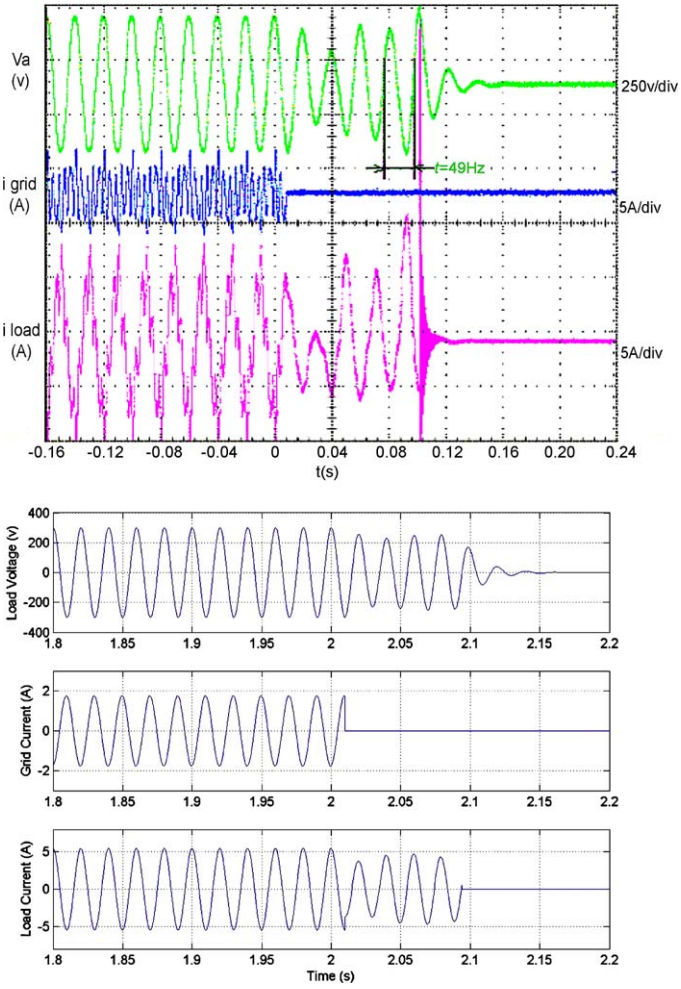

Fig. 20. Islanding detected by the SMS method in the case where P_{inv} is 33% less than P_{load}.

7.2. Computational experiment 2

In this experiment, we aim at comparing detection times in a situation where both the standard OUV/OUF method and the SMS method can detect islanding.

Both these methods were tested under real power mismatched conditions, which were taken as follows:

- DC power: $P_{DC} = 2.6\ A \times 233\ V \approx 606\ W$,
- The power of the load: $P_{load} = (212\ V)^2/55\ \Omega \approx 817\ W$,
- The output power of the inverter: $P_{inv} = P_{DC}(1 - 0.08) \approx 558\ W$,
- Degree of imbalance: $\Delta P/P_{load} = 558\ W - 817\ W/817\ W \approx -32\%$.

Under these conditions, both methods can detect islanding. However, the efficiency of the SMS methodology is higher and, as shown in Fig. 20, experimental and simulation results for this method are in good agreement. It takes $(0.102 - 0.008) = 0.094$ s to detect the islanding by the SMS method. This is by 0.03 s less (or 33% less) compared to the standard OUV/OUF methodology. The efficiency of the SMS makes it a method of choice in real power mismatched situations. It is a reliable methodology, which outperforms standard methodologies such as the OUV/OUF method.

8. Conclusions

In this paper, we developed models and their SIMULINK implementations for two representative examples of the most effective methodologies from passive and active groups of methods. Our choice was based on an overview of the existing methodologies for islanding detection. By analyzing non-detection zones of these methods and comparing them with non-detection zones of the standard methodologies such as OUV/OUF, we came to the conclusion that the SMS method stands out of the methods we analyzed here. It has a simple theoretical justification, a relatively easy (low cost) implementation, and a good output power quality. The results of computational experiments, based on the model with built-in SMS methodology, agree well with those obtained by experiments. Even if powers are closely matched and most of standard methodologies fail to predict islanding, the SMS method can reliably detect islanding conditions within 0.2 s, as required by the IEEE standards [2]. When standard methodologies, such as the OUV/OUF, can detect islanding, the SMS methodology can do that more reliably and quicker. Computational experiments show that in some cases, this advantage can lead to a 33% faster detection time with the implementation of the SMS methodology.

References

[1] Hopewell PD, Jenkins N, Cross AD. Loss-of-mains detection for small generators. IEE Proceedings: Electric Power Applications 1996;143(3):225–30.

[2] IEEE Standards Coordinating Committee 21 on Fuel Cells, Photovoltaics, dispersed generation, and energy storage. IEEE Recommended Practice for Utility Interface of Photovoltaic (PV) Systems (IEEE Std 929-2000 (revision of IEEE Std 929-1988)); 2000. p. 3–20.
[3] Ishida T, et al. Anti-islanding protection using a twin-peak band-pass filter in interconnected PV systems and substantiation evaluations. IEEE First WCPEC: World Conference on Photovoltaic Energy Conversion. 1994. p. 1077–80.
[4] Kobayashi H, Takigawa K. Statistical evaluation of optimum islanding preventing method for utility interactive small scale dispersed PV systems. First WCPEC, IEEE. 1994. p. 1085–6.
[5] Kobayashi H, et al. Method for preventing islanding phenomenon on utility grid with a number of small-scale PV systems. 22 IEEE Photovoltaic Specialists Conference, vol. 1. 1991. p. 695–700.
[6] Kobayashi H, Takigawa K. A new protective method for grid connected dispersed PV systems to detect short circuit fault in distribution line. Solar Energy Materials and Solar Cells 1997;47:117–23.
[7] Kroposki B, Ye Z, Miller N, Walling R, Delmerico R. Reliable low cost distributed generator/utility system interconnected. DOE Distributed Power Program Quarterly Review Meeting, July 9–10, 2002 Madison, WI. 2002 http://www.eere.energy.gov/distributedpower/pdfs/review1q_02pres/1q02_23ge.pdf.
[8] Okado C, et al. A novel islanding protection system for photovoltaic inverters. Electrical Engineering in Japan 1995;115(4):60–70.
[9] O'Kane P, Fox B. Loss mains detection for embedded generation by system impedance monitoring. IEE Conference on Developments in Power System Protection, London, England. 1997. p. 95–8.
[10] Onions PA, Smith GA. Anti-islanding protection of grid connected PV inverters. 34th Universities Power Engineering Conference, vol. 2. 1999. p. 378–72.
[11] Pai F-S, Huang S-J. A detection algorithm for islanding-prevention of dispersed consumer-owned storage and generating units. IEEE Transactions on Energy Conversion 2001;16(4):346–51.
[12] Redfern MA, Barrett JI, Usta O. A microprocessor based islanding protection algorithm for dispersed storage and generation units. IEEE Transactions on Power Delivery 1995;10(3):1249–54.
[13] Redfern MA, Usta O, Fielding G. Protection against loss of utility grid supply for a dispersed storage and generation unit. IEEE Transactions on Power Delivery 1993;8(3):948–54.
[14] Ropp ME, Begovic M, Rohatgi A. Analysis and performance assessment of the active frequency drift method of islanding prevention. IEEE Transactions on Energy Conversion 1999;14(3):810–6.
[15] Ropp ME, Begovic M, Rohatgi A. Prevention of islanding in grid-connected photovoltaic systems. Progress in Photovoltaics: Research and Applications 1999;7:39–59.
[16] Smith GA, Onions PA, Infield DG. Predicting islanding operation of grid connected PV inverters. IEE Proceedings—Electrical Power Applications 2000;147(1):1–6.
[17] Takigawa K, Kobayashi H. A development of compact and reliable protective control unit for grid connected small residential PV systems. IEEE First WCPEC: World Conference on Photovoltaic Energy Conversion. 1994. p. 1081–4.
[18] Tsukamoto O, Okayasu T, Yamagishi K. Study on islanding of dispersed photovoltaic power systems connected to a utility power grid. Solar Energy 2001;70(6):505–11.
[19] Yuyama S, et al. A high speed frequency shift method as a protection for islanding phenomena of utility interactive PV systems. Solar Energy Materials and Solar Cells 1994;35:477–86.